BBA - Bioenergetics 1862 (2021) 148395

Contents lists available at ScienceDirect

BBA - Bioenergetics

journal homepage: www.elsevier.com/locate/bbabio

Duplexing complexome profiling with SILAC to study human respiratory chain assembly defects

Petra Páleníková [a], Michael E. Harbour [a,1], Federica Prodi [b], Michal Minczuk [a], Massimo Zeviani [a,2], Anna Ghelli [b], Erika Fernández-Vizarra [a,*]

[a] Medical Research Council-Mitochondrial Biology Unit, University of Cambridge, Cambridge, UK
[b] Dipartimento di Farmacia e Biotecnologie (FABIT), Università di Bologna, Bologna, Italy

ARTICLE INFO

Keywords:
Quantitative proteomics
SILAC
Mitochondrial DNA mutations
Mitochondrial disease
Complex III
Complex IV

ABSTRACT

Complexome Profiling (CP) combines size separation, by electrophoresis or other means, of native multimeric complexes with protein identification by mass spectrometry (MS). Peptide MS analysis of the multiple fractions in which the sample is separated, results in the creation of protein abundance profiles in function of molecular size, providing a visual output of the assembly status of a group of proteins of interest. Stable isotope labeling by amino acids in cell culture (SILAC) is an established quantitative proteomics technique that allows duplexing in the MS analysis as well as the comparison of relative protein abundances between the samples, which are processed and analyzed together. Combining SILAC and CP permitted the direct comparison of migration and abundance of the proteins present in the mitochondrial respiratory chain complexes in two different samples. This analysis, however, introduced a level of complexity in data processing for which bioinformatic tools had to be developed in order to generate the normalized protein abundance profiles. The advantages and challenges of using of this type of analysis for the characterization of two cell lines carrying pathological variants in *MT-CO3* and *MT-CYB* is reviewed. An additional unpublished example of SILAC-CP of a cell line with an in-frame 18-bp deletion in *MT-CYB* is presented. In these cells, in contrast to other MT-CYB deficient models, a small proportion of complex III_2 is formed and it is found associated with fully assembled complex I. This analysis also revealed a profuse accumulation of assembly intermediates containing complex III subunits UQCR10 and CYC1, as well as a profound early-stage complex IV assembly defect.

1. Introduction

1.1. Complexome profiling general overview

The structural and functional characterization of multi-heteromeric protein complexes, often embedded in a phospholipid bilayer membrane, such as the complexes of the oxidative phosphorylation system (OXPHOS), is still a big challenge for structural biology. Although the development of cryo-EM has now made available several complex structures which were previously uncharacterized due to unsucessful crystallisation attempts, the access to the necessary instrumentation and bioinformatic tools, as well as the possibility to analyze certain samples, such as patient-derived material is still more than a challenge. Therefore, the powerful and elegant approach based on Cryo-EM should be complemented with a set of strategies, mostly based on identification of protein interactors through different proteomic-based analysis exploiting as much as possible techniques that maintain the complexes in their native conditions, particularly of multiprotein and membrane bound structures, such as complexome profiling (CP).

CP is a comprehensive proteomic tool used mainly for the analysis of membrane-associated, multimeric complexes in organelles from the cells of various eukaryotic species, as well as bacteria (see the articles in this issue). It was initially developed for the study of the OXPHOS complexes, the multimeric enzymes present in the mitochondrial inner membrane responsible for ATP production. The OXPHOS system is composed of four respiratory chain complexes (complexes I-IV) and the

* Corresponding author at: Institute of Molecular, Cell and Systems Biology, University of Glasgow, Glasgow, UK.
E-mail address: Erika.Fernandez-Vizarra@glasgow.ac.uk (E. Fernández-Vizarra).
[1] Present address: STORM Therapeutics LTD, Babraham Research Campus, Cambridge, UK.
[2] Present address: Venetian Institute of Molecular Medicine, Via Orus 2, Padua, Italy; Department of Neurosciences, University of Padua, via Giustiniani 2, Padua, Italy.

https://doi.org/10.1016/j.bbabio.2021.148395
Received 16 December 2020; Received in revised form 3 February 2021; Accepted 5 February 2021
Available online 16 February 2021

ATP synthase or complex V. It is now clear that the respiratory chain complexes interact with each other, where dimeric complex III ($cIII_2$) binds with complexes I and IV forming 'supercomplexes' of variable stoichiometry, whereas complex V forms dimers through the interaction of the membrane domains [1,2]. In human cells, almost all of complex I (cI) is found associated in supercomplexes [3]. Most of this information has been gathered using Blue-Native gel electrophoresis (BN-PAGE) in which intact membrane-associated complexes are extracted with non-ionic detergents and separated electrophoretically in their native state [4–6].

CP increases the analytical possibilities by combining the separation technology of BN-PAGE with the protein identification capabilities of peptide mass spectrometry (MS). Prior to the development of CP, the assembly state and levels of the OXPHOS complexes were usually assessed either by detecting the presence of native electrophoresis bands containing the active enzymes, technique known as 'In-gel-activity (IGA)' assays [7] or by Western blotting of the BN-PAGE and immunodetection using antibodies raised against individual OXPHOS components [5]. However, there are no available antibodies for each and every one of their structural subunits and ancillary factors. The unbiased and high-throughput character of MS has provided essential information about the modular nature of the assembly of respiratory complexes [8] as well as the composition of assembly intermediates that was essentially missed with other protein detection methods.

In the past, attempts to analyze the protein composition of single complex bands, vi visualized by dye staining and excised from BN-PAGE gels, had failed because the sensitivity of the spectrometer results in the detection of large numbers of unexpected proteins. It was impossible to determine whether these proteins were real interactors of the complex contained in the band or merely 'background' proteins detected due to the imperfect resolution of the electrophoretic separation. In contrast, in CP the entire electrophoresis gel lane is analyzed by being divided into thin portions where each one is subjected to peptide MS analysis. Protein lists obtained from single bands are replaced with peptide profiles from the entire gel lanes enabling the determination, after normalization, of the peaks for maximum protein abundance along the electrophoretic separation lane [9–11]. Migration of proteins at molecular sizes greater than their calculated individual masses suggests binding interactions, and co-localization of proteins in the same intensity peaks make them very likely to be part of the same molecular complex. Appearance of a protein in multiple fractions in a lane could suggest the presence of the protein as part of multiple complexes of different composition or in assembly intermediates, different oligomeric states or an equilibrium between bound and free states. However, such appearances need to be interpreted with caution as some degree of artefactual complex dissociation can be due to detergent treatments of the mitochondrial membranes. In addition, there are several challenges in the analysis and interpretation of MS-derived CP data that will be discussed below (Section 2.3.1). Nonetheless, the development of CP has provided an extremely useful and cost- and time-effective way to characterize the protein composition and organisation of the human OXPHOS system components in different pathological cell models, as well as the determination of respiratory complex assembly pathways and the identification of chaperones involved in these pathways [9,12–22].

1.2. Use of SILAC for duplexing in CP

Protein profiles generated by CP are dependent on the electrophoretic migration of the complexes in BN-PAGE, which can be highly variable among different gels and occasionally even between two lanes in the same gel. Furthermore, there are obvious practical difficulties in the manual slicing of different gel lanes into many lots of thin pieces in which the lack of accuracy can result in profile mismatches. Therefore, comparison of the complex assembly status between separate control and treatment samples can suffer from artefacts. The differences in migration can be overcome by using the COmplexome Profiling ALignment (COPAL) tool, developed for this purpose [16]. However, sequential MS analysis of the two compared biological samples, each divided into 60–64 separate fractions, still represents a suboptimal use of resources and a further opportunity for introducing undesirable artefactual variation. In addition, since the normalization of peptide abundance can only be done within the same sample/BN-PAGE lane (see Section 2.3.1), the quantification of the relative amounts of the same protein between two independently samples is not possible. However, such quantitative comparison is often desired as protein abundance variations between a pathological and a control sample provide very relevant information to better understand the assembly defects associated with OXPHOS deficiencies.

For these reasons, we decided to introduce the well-established 'stable isotope labeling of amino acids in cell culture' or 'SILAC' technology [23,24] into our CP pipeline (SILAC-CP). In this way, we subject the two differentially metabolically labeled samples to the same conditions of mitochondrial isolation, solubilization and electrophoresis, manual gel-piece fraction cutting, proteolytic digestion, chromatography and MS. Furthermore, by combining SILAC technology with CP approaches we have been able to directly compare respiratory chain supercomplex, complex and subcomplex migration as well as abundance in a series of defective cell lines and their appropriate controls [14,21,25] (Fernandez-Vizarra et al., in this issue).

In this article we review a few studies in which SILAC-CP has been used, highlighting the usefulness of introducing SILAC proteomics to directly compare the migration and abundance of the OXPHOS complexes in pathological cell lines (specifically *MT-CO3* or *MT-CYB* mutants) vs. controls, also pointing out the caveats and challenges encountered during the analysis of the dual-labeling datasets. As an additional example, we present an unpublished SILAC-CP analysis performed in cytoplasmic hybrid (cybrid) cells carrying an in-frame 18-bp deletion in the mitochondrial DNA (mtDNA) gene encoding the complex III subunit *MT-CYB*, in comparison with its isogenic wild-type (WT) control [26,27].

2. Methodological overview

2.1. Labeling and preparation of the samples for native electrophoresis

The two cell lines to be compared, for example, control (C) and mutant (M), are grown in DMEM medium for SILAC (ThermoFisher Scientific) lacking the amino acids Arg and Lys. The 'Heavy (H)' medium is supplemented with dialysed foetal bovine serum (D-FBS; Gibco) and the amino acids labeled with heavy stable isotopes of carbon and nitrogen (Sigma-Aldrich): L-lysine- $^{13}C_6$, $^{15}N_2$ (K_8) and L-arginine- $^{13}C_6$, $^{15}N_4$ (R_{10}). Unlabeled proline is also added to prevent the conversion of heavy arginine to proline [28]. The 'Light (L)' medium is prepared in the same way except for the K and R amino acids, which are the ^{12}C and ^{14}N-containing ones (K_0 and R_0). Both cell lines are kept separately in H and L media and grown, at 37 °C in a 5% CO_2 humidified incubator, for eight passages to guarantee the complete labeling of the whole proteomes. Before proceeding with the experiments, the extent of the H labeling is verified by analyzing a total cell protein extract by mass spectrometry and determining the H to L peptide ratios from representative proteins.

The results of the SILAC-CP are usually based on duplicate experiments in which the labeling is reversed, i.e., one experiment with L-labeled C cells and H-labeled M cells; whereas the second experiment is with H-labeled C cells and L-labeled M cells [29] (Fig. 1). Once the complete incorporation of the H labeling is achieved, the cells are expanded in their corresponding SILAC medium. The differentially labeled M and C cells, each contained in five 150-mm plates, are mixed in a 1:1 proportion. The mixed cellular pellet can be frozen at −80 °C before the mitochondrial extraction. Next, mitochondria are isolated from the fresh or frozen cells using a homogenization and differential centrifugation procedure [30]. The complexes are extracted from the mitochondrial membranes without delay using a mild anionic detergent,

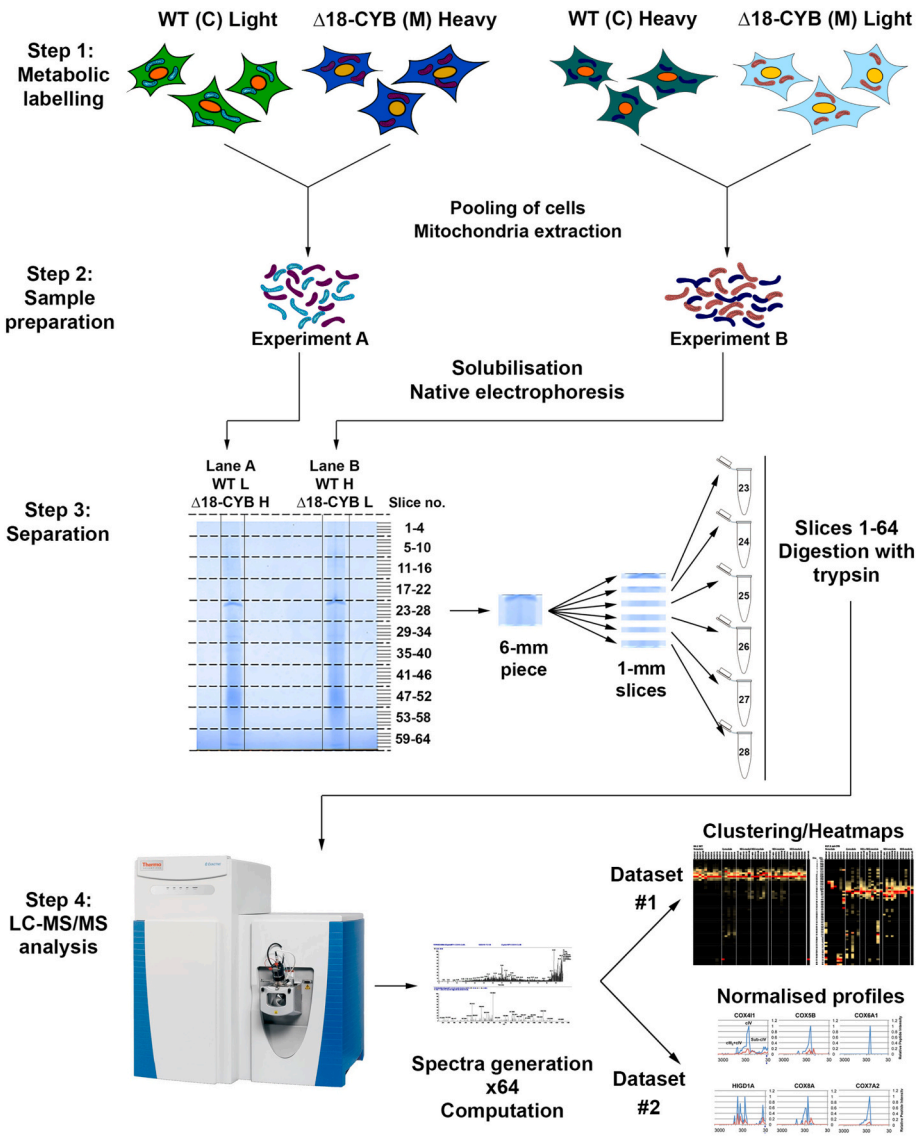

Fig. 1. SILAC-Complexome Profiling workflow: analyses start with SILAC labeling of the two cell lines with 'heavy (H)' and 'light (L)' amino acids in culture. This allows to obtain the samples to perform the two 'reciprocal' experiments. Differentially labeled cells are mixed in a 1:1 ratio and mitochondrial isolation is performed. Mitochondrial membranes are then solubilized, and the native electrophoresis is carried out. Once the samples are separated and the gel is stained, each lane, containing one of the differentially labeled duplicates, is excised in 64 slices and these are processed and analyzed by LC-MS/MS. After peptide identification, the computational analysis is done to generate the datasets used to build the complexome profiles (see main text for details).

which can be either 1.6 mg n-dodecyl-β-maltoside (DDM)/mg of mitochondrial protein, to separate the individual complexes from the supercomplexes [14,31,32], or digitonin to maintain the interactions within the supercomplexes [1,6]. Our standard protocol uses a digitonin to protein ratio of 4:1 [21], which is the middle point in the optimal range of 2 to 8 mg/mg determined for mammalian mitochondria to isolate the respiratory supercomplexes [1,6,17,32–35]. The extracted fractions are separated by electrophoresis on a native gel in the presence of Coomassie Blue G-250, as described [6,32,36]. In order to ensure migration reproducibility, we use precast commercial native gels and run the two reciprocally labeled samples in two lanes of the same gel (Fig. 1). The electrophoresis is left to proceed for approximately 16 h at low voltage (40 V) in the cold room, and once the front has reached the end of the gel the run is stopped. The gel is then stained for 30 min with a solution containing 0.2% Coomassie Blue R-250, 50% methanol and 7% Acetic Acid. Subsequently it is de-stained in 20% methanol and 7% acetic acid for 2–3 h with frequent changes. Once the background colour is eliminated from the gel, each lane is cut in sixty-four ~1 mm-thick slices. To do this, we use a transparent gridline template where the lines are 6 mm apart from each other (Fig. 1). The gel is placed over the gridline on a transilluminator, using the Coomassie stained complex bands as the reference for positioning. Using a scalpel, the lane to be cut is separated from the rest of the gel and then excised into eleven 6-mm pieces. Each one of these pieces is then divided in six equal slices of 1 mm each. The top two slices are discarded, giving the total of sixty-four slices.

2.2. Digestion and mass-spectrometry

Each gel slice is placed in a clean Eppendorf tube pre-rinsed with 50% HPLC-grade methanol. The slices are kept at −20 °C until further processing. Slices are washed in a buffer mix (BM) of 20 mM Tris-HCl (pH 8), then in a 50:50 mix of BM with acetonitrile (ACN), and finally chemically dehydrated in 100% ACN. The ACN is taken off and gel pieces are dried to completion in a SpeedVac drier. Desiccated pieces are then digested with 4–10 μl of working trypsin solution (BM, 5 mM $CaCl_2$, 12.5 ng/μl Trypsin) to cover and rehydrate them. Digestion takes place for 4 h or overnight at 37 °C in an oven.

After digestion, approximately 10 μl of a 'peptide extraction solution' of 60% ACN, 4% formic acid is added to the digested slices. Samples are spun heavily to sediment particulate matter and the liquid phase is transferred to complete-recovery bottles for mass-spectrometry. Given the nature and importance of relative comparisons to the SILAC-CP assay, great care during sample handling is taken to treat all 64 gel slices in exactly the same way.

Although LC-MS/MS spectrometer instrumentation and analysis

parameters will vary depending on the facility, a typical setup is described. For each sample analysis, the results of the digestion and extraction are loaded onto a reverse phase column (75 μm i.d. x 100 mm; Nanoseparations) and chromatography (buffers A and B, 5% and 95% aqueous acetonitrile, respectively, each containing 0.1% formic acid) is performed with a gradient of 0–40% buffer B over 84 min with a flow rate of 300 nl/min. The eluent is passed into an LTQ OrbiTrap XL mass spectrometer (Thermo Fisher) operating in data-dependent MS/MS mode, with a mass scan range of 400–2000 Da for precursor ions and MS/MS of the top 10 highest abundance ions are selected from the full scan, for fragmentation by CID with nitrogen, during each instrument duty-cycle.

2.3. Data analysis

2.3.1. Technical considerations for the analysis of MS data in a CP experiment

Absolute quantification of peptide abundance with MS is not currently possible without sophisticated protocols involving either the addition of known amounts of synthetic peptide controls and the generation of standard curves or the use of complicated and not entirely validated bioinformatic algorithms for label-free quantification [37,38]. The comparison of the abundance of peptides with different molecular composition is complicated because the observed MS signal does not only depend on the amounts of the parent protein in the original biological sample, but is also a function of the unique combination of: i) efficiency of proteolytic digestion, ii) recovery during the process of reverse-phase-chromatographic separation required to introduce sample to the spectrometer, iii) efficiency of ionisation during the electrospray process and iv) the degree to which the available quantity of that peptide divides into subpopulations of different ionic charge states and oxidation states.

Analysis of CP experiments relies on the following assumptions. First, that at least some meaningful comparison of relative abundance can be made between signals obtained from the same peptide 'species' of a specific mass-to-charge (m/z) ratio and oxidation state. Second, that the samples are handled and prepared manually as similarly as possible and analyzed sequentially in the same batch-run of a spectrometry session. Under such conditions, the variation introduced by confounding factors are minimized to a great degree. The expectation is that differences in peptide intensity within the collection of fractions derived from the same original sample do reflect genuine abundance changes of a single protein along the electrophoretic separation lane and together constitute a profile for that protein. The arbitrary 'ion count' measures for the peptides have little meaning and can be highly variable between different experiments, therefore, normalization for each peptide is performed by scaling the values such that the highest number in the whole profile is set to unity. A common approach is to make the estimation of protein abundance using the average of the three peptides with the highest ion counts originating from that protein. Once profiles for relative protein abundances in the gel lane have been acquired, hierarchical clustering can be performed to group and order them by similarity. A variety of similarity metrics could be employed, the most commonly used being the Pearson Uncentered Correlation Coefficient. The results of clustering can be visualised with a coloured scale 'heatmap', optionally with an accompanying similarity dendrogram to reveal the protein complexes with similar migration [9,11].

2.3.2. Duplexed data processing

The incorporation of SILAC to allow sample duplexing and comparison of protein relative abundance in CP involves: i) the isotopic labeling of cells at the outset, ii) the mixing of whole cells after labeling but prior to solubilization and BN-PAGE and iii) the bioinformatic de-duplexing of the raw data after acquisition. Incorporation of SILAC into CP required adjustments in data processing. Due to the added level of complexity in the SILAC-CP data by incorporation of the heavy isotopes in the peptides, and to allow a reliable comparison of the relative protein amounts in the labeled and unlabeled samples, we use an alternative approach for protein abundance estimation based on the ion counts from a single representative peptide rather than the 'average-of-top-three' approach. This 'single-peptide' system has still provided a meaningful way of analyzing the data for the purpose of creating complexome profiles using duplexed data.

For the analysis of SILAC-CP data we used a combination of commercial software and custom Python and R scripts. First, raw mass spectrometry data were analyzed using the Proteome Discoverer software (PD, Thermo Fisher). PD was used for: i) coordination of protein identification with the Mascot peptide search engine (Matrix Science), ii) peptide quantification and iii) export of peptide identity and intensity data to a plain text file. Mascot was configured to consider the possibility of the presence of the appropriate H-labeled amino acid residues. The peptide data produced by PD were then analyzed using custom Python and R scripts.

First, a Python script was used to 'de-duplex' the peptide dataset, separating the information corresponding to the H-labeled and unlabeled (L) peptides. The script was written to generate two distinct pairs of datasets. Dataset #1 contains ion counts (or intensity data) of the most abundant peptide for each protein independently of the labeling state. Dataset #2 contains the information corresponding to the intensities of a representative peptide found in common in the two labeling states, which is the one that appeared in the greatest proportion of the total number of gel slices in both unlabeled (L) and labeled (H) forms. Hence, this was the peptide for which the greatest number of L vs. H intensity comparisons could be made. Next, the Python script calculated peptide relative abundances for each protein of dataset #2 as a ratio between intensity value in each slice, and the value in the slice and labeling state with the highest intensity, which is set to 1. These data were used to create profile graphs, either with Microsoft Excel or GraphPad Prism, of relative peptide (or protein) abundance vs. either gel slice or molecular mass, calculated by regression analysis using the known molecular sizes of the OXPHOS complexes [14,21] (Figs. 2, 3 and 4). The Y-axes of these graphs have been labeled as "relative peptide intensity" instead of "relative protein abundance", although both are considered correct in this case. Furthermore, these profiles have been used to estimate the relative amounts of the protein by calculating the area under the curve (AUC) in the graphs generated by plotting relative peptide abundance vs. slice number (Fig. 3). The validity of these estimations was confirmed by independent quantification methods, i.e. direct calculation of the protein H/L ratios in the whole samples (not considering the separation into slices) and Western-blot and immunodetection of the proteins [21].

Further, the R scripts were written for normalization and hierarchical clustering, which can be done with either dataset #1 or #2. The R scripts normalized the protein abundances to the highest ion count in each labeling state separately. The clustered profiles were visualized into 'heatmaps' using Microsoft Excel. We provide examples of heatmaps generated in this way using the information contained in 'dataset #1', i.e. analyzing each labeling state separately (Fig. 2).

The data analyses performed as described above required significant manual input from the user in several of the steps. To facilitate the procedures, a ComPrAn R-package was recently developed to streamline the analysis. ComPrAn integrates all analysis steps, provides dedicated visualization functions and graphical user interface. For a detailed explanation of the analysis steps and a description of ComPrAn, see Páleníková, et al. in this issue.

2.4. Pitfalls and limitations of the method

SILAC-CP as described herein can only be applied to cells in culture that proliferate well , which is a limitation when trying to analyze post-mitotic tissues or even primary cells. Severe OXPHOS mutant cell lines that require a richer medium could also constitute a problem when

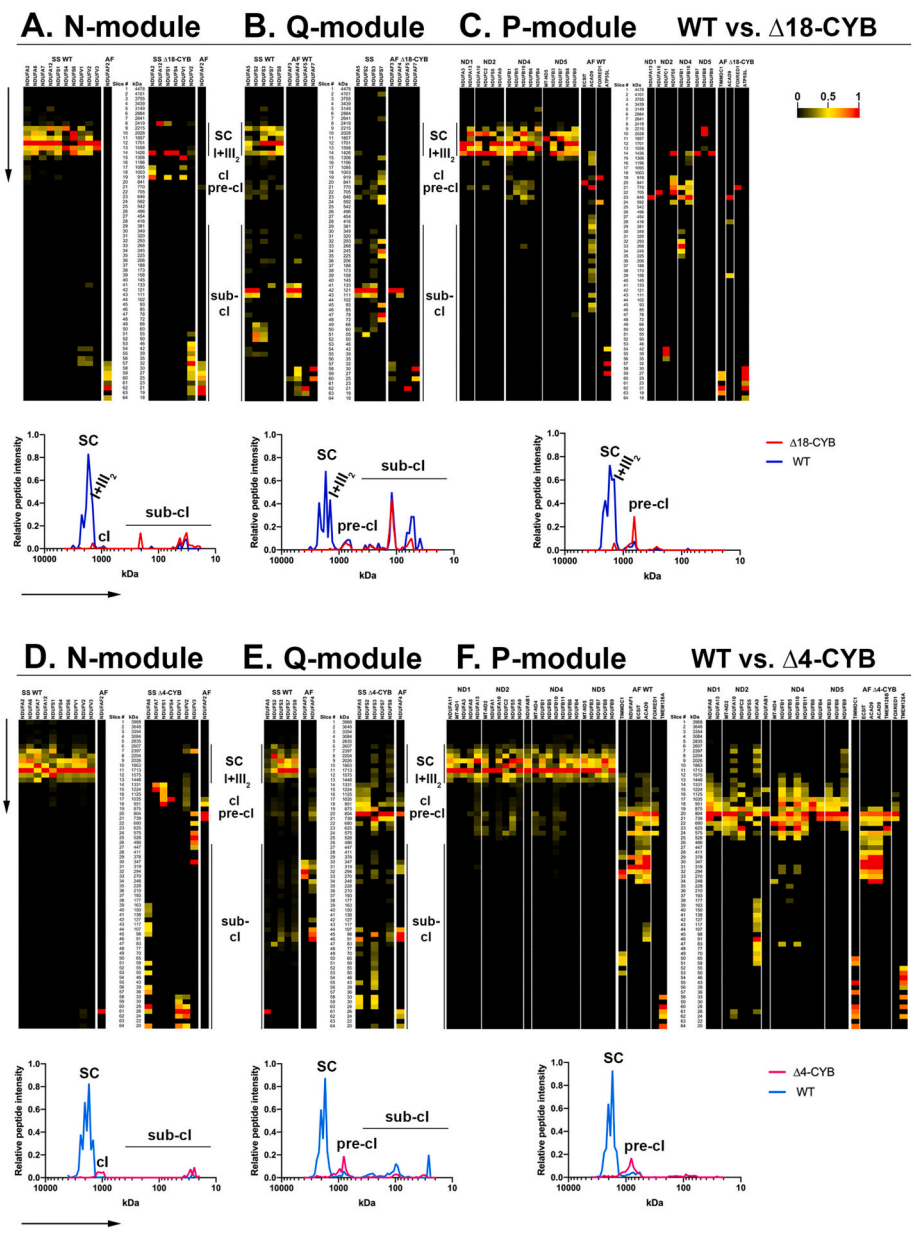

Fig. 2. SILAC-CP analysis of cI subunits in the Δ18-CYB cells and Δ4-CYB cells in comparison with their isogenic WT control cybrids. Heatmaps and complexome profiles generated by representing the normalized peptide intensities of the detected complex I structural subunits (SS) and assembly factors (AF) associated with the (A, D) N-module, (B, E) Q-module and (C, F) P-module, derived from the analysis of one of the reciprocal labeling experiments containing Light WT and Heavy Δ18-CYB samples (A, B and C) and Light WT and Heavy Δ4-CYB samples (D, E and F). The heatmaps were created with 'dataset #1' analyzing separately the most frequently found peptide, representative of the subunit or assembly factor, in each labeling state. The line graphs were created using 'dataset #2' where the intensity values of the common peptides for each protein were normalized to the maximum intensity within the two labeling states. The profiles represent the average normalized (relative) peptide intensities of all the detected structural subunits corresponding to each one of the cI modules, in function of their apparent molecular mass (kDa). The arrows indicate the direction of the electrophoresis, from high to low molecular size. SC: supercomplexes (mainly those formed of I + III_2 + IV); I + III_2; supercomplex formed by the association of complexes I and III_2 (ca. 1400 kDa); pre-cI: advanced subcomplex of ~830 kDa lacking only the N-module; sub-cI: subassembled species of lower molecular mass than mature cI (<1000 kDa) and pre-cI.

trying to apply this method for their analysis. Alternative media formulations, such as DMEM:F12 mixtures for SILAC, are available commercially and are helpful in some occasions to overcome this problem [25].

SILAC labeling offers multiplexing of only a limited number of samples. Use of 'heavy' and 'light' amino acids allows only duplexed analyses, which is enough if the aim is to compare one mutant cell line vs. one control. 'Medium' labeling amino acids are also available in the case the simultaneous analysis of a third sample is needed, however this is the limit of the 'traditional' SILAC multiplexing capacity. The use of NeuCode labeling would increase the multiplexing capacity of the method and it has the advantage that if using only different 'heavy' Lys varieties there is no need to achieve 100% protein metabolic labeling [39,40]. This opens up the possibility for the analysis of slowly proliferating cells or even post-mitotic tissues from animal models. However, the MS analysis of this kind of labels requires high resolution instrumentation that is not accessible for every facility. Another possibility to increase the multiplexing capacity (up to 16plex) and to be able to use low-proliferating cells or tissues, is to use chemical labeling such as Tandem Mass Tag (TMT) systems [41], where the proteins are labeled after they are extracted and then the samples are mixed right before the MS analysis. However, whenever possible we prefer the metabolic differential labeling that allows mixing the cells before sample processing, guaranteeing the same mitochondrial and protein yields in the two samples to be compared. This eliminates possible artefacts in the quantification process derived from differences between the samples in mitochondrial yield, protein extraction and labeling efficiency.

Whenever sample multiplexing is employed, it is critical that the protein quantification method used to determine cell quantities is accurate and reliable because mixing exactly the same amount of protein of each cell line is crucial for the experiment outcome. The equal mixing of the cells can be tested by determining the abundance, through calculation of the H/L ratios, of the bulk of the proteins present in the total sample [21] (Fig. S1A and B). If the majority of the proteins display logarithmic ratios of around zero, that provides a good indication that the original cell samples were correctly mixed (Fig. S1B). Another useful indication of the quality of the experiment is the distribution of the data for the same protein in the duplicate experiments. By plotting the $\log_2$

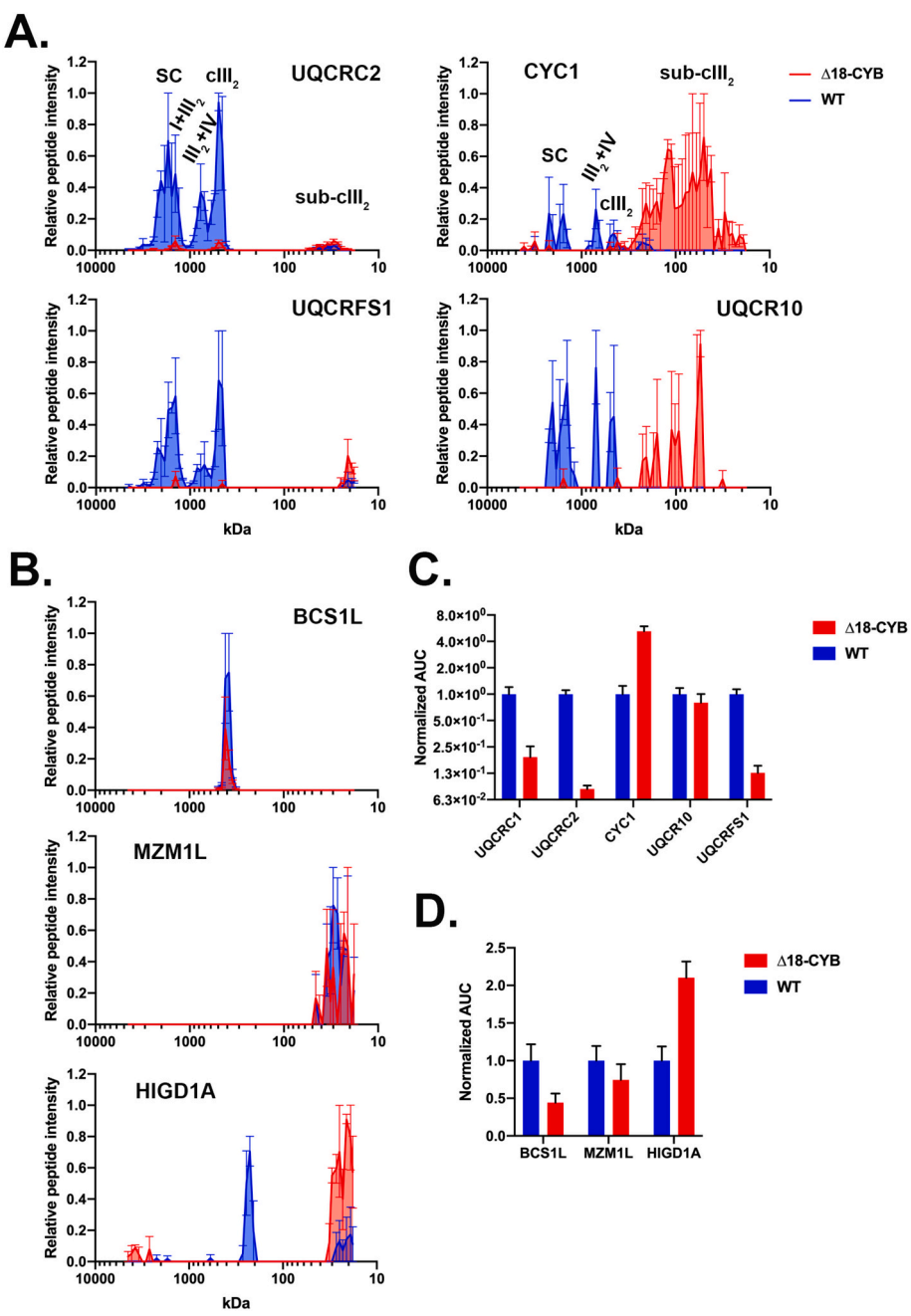

Fig. 3. Relative distribution and abundance of $cIII_2$ structural subunit and assembly factors in Δ18-CYB cells in comparison with their isogenic WT control cybrids. (A) SILAC-CP analysis generated with the normali zed (relative) common peptide intensity values of $cIII_2$ structural subunits UQCRC2, UQCRFS1, CYC1 and UQCR10. The values in the graphs are the mean ± SEM of the normalized peptide intensities derived from datasets #2 of the two samples from the duplicate reciprocal labeling experiments, separated in the same gel, in function of their calculated molecular size (kDa). (B) Complexome profiles generated in the same way as in (A) corresponding to the detected $cIII_2$ assembly factors BCS1L, MZM1L and HIGD1A. (C) Estimation of protein abundance by quantification of the total peak area under the curves (AUC) defined by the peptide intensity peaks for the indicated $cIII_2$ subunits. The x-axis values were the slice number (1–64), and the y-axis values were the relative peptide intensity. The AUC values for each protein were normalized to that of the WT. The graph shows the mean ± SEM ($n = 2$). (D) Protein abundance calculated as the normalized AUC for the indicated $cIII_2$ assembly factors, calculated as in panel C. The graph shows the mean ± SEM (n = 2). SC: supercomplexes I + III_2 + IV and I + III_2 (the peak at ~1400 kDa corresponding to SC I + III_2 is specifically indicated); III_2 + IV: supercomplex formed by the association of dimeric complex III ($cIII_2$) and complex IV; sub-$cIII_2$: subassembled species of lower molecular mass than mature $cIII_2$ (<485 kDa).

H/L ratios of each experiment in the x- and y-axis of a graph, respectively, most of the proteins should gather in the axis origins and the differentially expressed proteins should distribute along an imaginary axis at a 45° angle, as shown in Fig. S1A. This indicates the correct mixing of the samples and the reproducibility of the data in the reciprocal labeling experiments. One concern that can arise, especially when analyzing mitochondrial disease samples, is that there could be differences in mitochondrial content with respect to the controls. This can be evaluated by determining the relative abundance of mitochondrial mass marker proteins, such as TOMM20, TOMM22 or citrate synthase (Fig. S1C).

Software tools and pipelines for MS data analysis different than Proteome Discoverer could be employed for SILAC-CP, as long as they provide data of peptide identity and quantity/intensity. However, the MaxQuant calculations of H/L protein ratios in each individual slice cannot be used because the information about the relative amounts of the same H or L-labeled peptide among all the analyzed fractions, necessary to construct the complexome profiles, would be lost.

When interpreting SILAC-CP data, it is important to point out that when comparing two different proteins, correlation of abundance profiles informs only about protein co-migration. Investigations of protein stoichiometry within the same complex are not possible because direct abundance comparisons between different peptide ‘species’ cannot be made due to the way the relative intensities are determined and normalized (see Section 2.3).

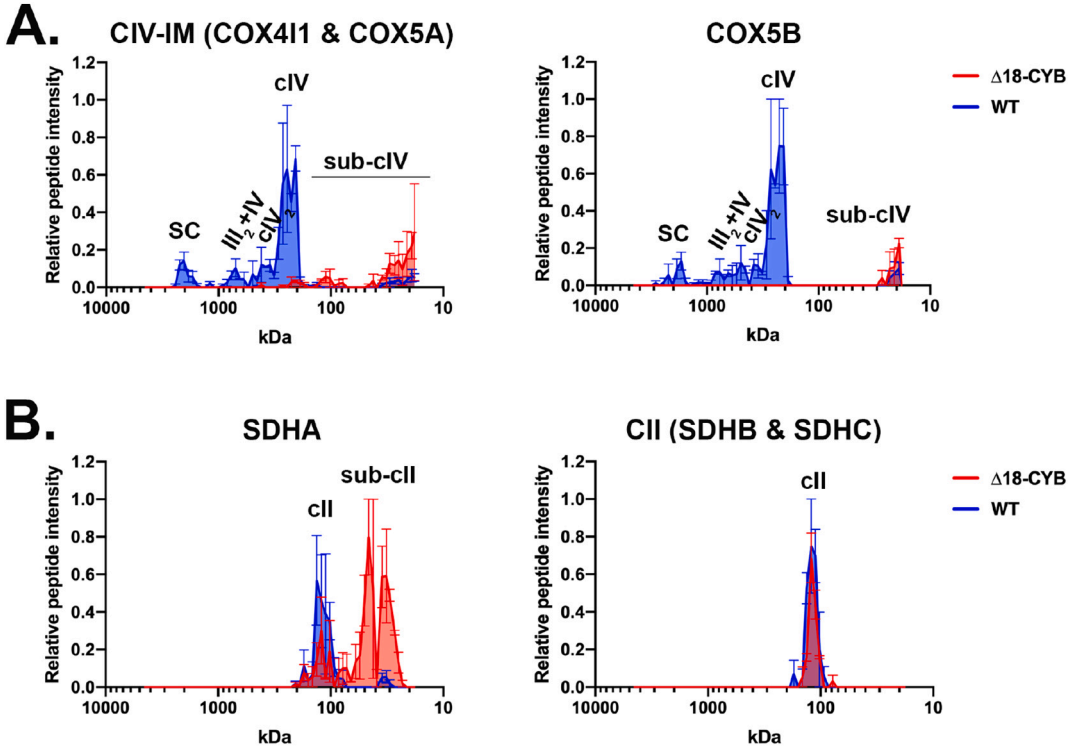

Fig. 4. Relative distribution and abundance of cIV and cII structural subunits in Δ18-CYB cells in comparison with their isogenic WT control cybrids. (A) SILAC-CP analysis generated with the normalized (relative) common peptide intensity values of (A) cIV and (B) cII structural subunits. The values in the graphs are the mean ± SEM of the normalized peptide intensities derived from datasets #2 of the two samples from the duplicate reciprocal labeling experiments, separated in the same gel, in function of their calculated molecular size (kDa). CIV-IM: complex IV initial module profile represented as the average of the normalized peptide intensity values corresponding to the COX4I1 and COX5A subunits. CII: complex II profile represented as the average of subunits SHDB and SDHC. SC: supercomplexes I + III_2 + IV; III_2 + IV: supercomplex formed by the association of dimeric complex III ($cIII_2$) and complex IV; cIV_2: dimer of cIV; sub-cIV: subassembled species of lower molecular mass than mature cIV (<214 kDa); sub-cII: subassembled species of lower molecular mass than mature cII (<123 kDa).

3. Usefulness of SILAC-CP for the analysis of cell lines with OXPHOS deficiency

3.1. Analysis of complex IV assembly intermediates in a cybrid cell line carrying a MT-CO3 pathological variant

The first time we combined CP with SILAC was for the analysis of cybrid cell line with a *MT-CO3* pathological variant. A virtually homoplasmic m.9537insC frameshift pathological variant in the mtDNA coding region for the cytochrome *c* oxidase (or complex IV) subunit *MT-CO3* was identified in an individual diagnosed with progressive spastic paraparesis, ophthalmoparesis and moderate mental retardation, presenting Leigh-like brain lesions [42]. Western blot and immunodetection analyses in cybrid cell lines bearing the mutation revealed that the steady-state levels of different complex IV (cIV) subunits were not affected equally, with COX4 and COX5A being comparable to controls, whereas COX6A and COX6B were drastically reduced [42]. The *MT-CO3* cybrids also displayed a profuse accumulation of cIV assembly intermediates containing MT-CO1 [14,42].

We performed proteomic analysis of cIV immunocaptured fractions of the mutated cells treated with SILAC in comparison with wild-type (WT) cybrids. This allowed us to determine the composition of the assembly intermediate species, the order of incorporation of the individual structural subunits and the identification of MR-1S (short isoform of *PNKD*) as cIV assembly factor [14]. SILAC-CP revealed the co-migration of MR-1S with PET100 and PET117 together with advanced cIV subassembled species lacking only the MT-CO3 module. The co-migrations of MR-1S with PET100 and PET117 as well as with structural cIV subunits, was confirmed by CP performed in different human primary and immortalised cell lines, and by co-immunoprecipitation analysis [14].

Use of SILAC-CP in this work highlighted the advantages of analyzing two different samples processed and electrophoresed together and led to the development of the analysis pipeline for duplexed data processing. It allowed us to visualise the migration profiles and relative abundance of each of the complexes, revealing the accumulation of the different subunits within stable assembly intermediates in both the physiological (WT cells) and pathological (*MT-CO3* mutant) conditions. We observed that the cIV subunits that are assembled first, such as COX4I1 and COX5A, were found at a range of molecular masses starting from low sizes up to the size corresponding to the mature complex. The relative abundance of these low molecular mass subassembled species was comparable in the mutant and WT cells, whereas the levels of fully assembled cIV were much lower in the MT-CO3 cybrids. The intermediate group of subunits were found located at intermediate positions in the gel lane and accumulated in the mutant, whereas the late incorporation 'MT-CO3 module' subunits (MT-CO3, COX6A1, COX6B1 and COX7A2) were only found in the peaks corresponding to holo-cIV and greatly reduced in the mutant cybrids compared to the controls [14]. The use of SILAC was crucial for the comparison of the amounts of MT-CO3 module subunits present within assembled cIV between the WT and the mutated cells. Without SILAC we would have found the maximum intensity of the late assembly proteins in fully assembled cIV in both cell lines, without the possibility of determining the extent of the assembly defect displayed by the MT-CO3 mutants. All in all, the data generated by SILAC-CP in this way were key for: i) determining the subunit composition of each of the accumulated sub-assembled species and ii) the refinement of the cIV assembly pathway from a linear to a modular fashion. In this model, COX4I1 and COX5A form an 'initial module' interacting with HIGD1A and the rest of the modules are defined by each

of the mtDNA-encoded cIV subunits (MT-CO1-3), and the MT-CO1 module is incorporated in the intermediate steps of the pathway [8,14].

3.2. Analysis of respiratory chain impaired biogenesis in cybrid cell lines carrying a frame-shift deletion in MT-CYB (Δ4-CYB)

We also applied SILAC-CP to perform a detailed analysis of the altered organization of the OXPHOS system in a cybrid cell line carrying a homoplasmic m.14787_14790delTTAA_CCAC mutation. The 4-bp deletion results in an early frameshift and absence of the encoded protein, the structural complex III ($cIII_2$) subunit MT-CYB. This mutation was identified in heteroplasmic state in a patient diagnosed with an overlap syndrome of Parkinsonism and MELAS (Mitochondrial Encephalopathy with Lactic Acidosis and Stroke-like episodes) [43]. Homoplasmic WT and mutated (Δ4-CYB) 143B cybrid clones were generated and selected from the patient's fibroblasts [44]. As in other cases of drastic impairment of MT-CYB synthesis, these cybrids showed severely impaired $cIII_2$ assembly (Fig. S2) and a secondary profound complex I (cI) deficiency (Fig. 2), with cIV being affected as well (Fig. S3) [21]. CI assembly proceeds in a modular fashion, where five modules (the Q-module and the four submodules of the P-module) are built independently and then joined together giving rise to a precursor known as 'pre-cI' or '830 kDa intermediate', only lacking the lastly incorporated catalytical N-module and stabilized by NDUFAF2 [13,45]. The thorough analysis provided by SILAC-CP, revealed a clear accumulation of the partially assembled cI modules in the Δ4-CYB cells (Fig. 2D-F). Also, significant amounts of stalled pre-cI containing NDUFAF2 were present in the mutated cells and absent in the WT cells (Fig. 2D). This indicated a stalling in the assembly of cI due to the absence of $cIII_2$ rather than its degradation once it is fully assembled, the other possibility that was proposed to explain the secondary cI deficiency caused by mutations in *MT-CYB* [21]. Further, estimation of protein levels by determining the area under the curve (AUC) of the complexome profile (the same way as in the graphs shown in Figs. 3C, D, S2C and D) showed that only around 5% of cI is found completely assembled, i.e. containing all five modules, and alone in the Δ4-CYB cells mutants compared to the total amounts of mature cI found in the WT cells. In the controls, circa 95% of cI was detected in the form of supercomplexes, that is, in association with complexes III_2 and IV [21]. These quantitative estimations and the observations that the levels and distribution of all cI subunits are not equally affected by the absence of $cIII_2$, were made possible by the introduction of SILAC in our CP analysis.

Regarding the assembly state of $cIII_2$ in the mutant cybrids, SILAC-CP revealed that the amounts of two subunits, CYC1 and UQCR10, were present in the mutated cells at similar levels to the WT, in contrast to other subunits which were greatly reduced. Both CYC1 and UQCR10 accumulated in different molecular size species (Fig. S2). This suggested their stabilization by interaction with each other and with other proteins, namely UQCRH and some cIV subunits, before they are incorporated into the nascent complex. This provides a change in the model explaining $cIII_2$ formation in human mitochondria, diverging from the assembly pathway proposed for the yeast enzyme [21,46–48].

3.3. Analysis of respiratory chain impaired biogenesis in cybrid cell lines carrying an in-frame deletion in MT-CYB (Δ18-CYB)

Here we present another example of SILAC-CP analysis used to study a different $cIII_2$-deficient model, a cybrid cell line homoplasmic for the m.15649_15666delATCCT_CCAT 18-bp in-frame deletion [26,27], in comparison with isogenic homoplasmic WT cybrids derived from the same patient. This variant was identified in heteroplasmy in an adult individual presenting a multisystem disease characterized by sensorineural deafness, cataracts, retinal pigmentary dystrophy, dysphagia, postural and gait instability and myopathy with exercise intolerance [26]. The main difference of this model with the previously analyzed Δ4-CYB, is that the 18-bp deletion occurs at the end of the *MT-CYB* coding sequence and results in an in-frame deletion of six amino acids (p. Ile300_Pro305del). This allows a certain proportion of the mutated protein to be synthesized and assembled into $cIII_2$ as well as the formation of supercomplexes [27] (Figs. S1, 2 and 3).

The duplicate samples obtained by mixing the reciprocally labeled WT and Δ18-CYB cells, as described in Section 2.1, were electrophoresed in two lanes of the same BN-PAGE, the gel was stained, and each lane excised in 64 slices (Fig. 1). The slices were processed and analyzed as described in Sections 2.2 and 2.3.

Fig. 2 shows the SILAC-CP results corresponding to the detected cI subunits in lane A of the gel, containing the L-labeled WT and H-labeled Δ18-CYB cells. The heatmaps were created with dataset #1, i.e., with the peptide intensity values of the most frequently found peptide independently of the labeling state. This analysis showed that fewer cI subunits were detected in the mutated sample (Fig. 2A-C), reflecting their lower abundance as a consequence of the secondary cI deficiency showed by this *MT-CYB* mutant [26]. For comparison, the graphs showing the profiles were generated from dataset #2, i.e., from the normalized intensities of the common peptides found in both labeling states for each cI subunit. The values for the proteins of each module were then averaged to create the complex profiles. These analyses indicated that the Δ18-CYB mutation also results in an accumulation of cI intermediates, because the relative amounts of subunits in the subassembled species are similar between the controls and mutated cells. However, the main difference between the Δ4-CYB model and the Δ18-CYB cybrids, is that the latter do not accumulate prominent amounts of pre-cI and only small amounts of NDUFA2 are found bound at a molecular size of around 800 kDa (Fig. 2A, left; compare with Fig. 2D). In addition, small but clearly detectable levels of supercomplex (SC) are being formed in these cells, consistent to what was found by Western blot and immunodetection analyses [27].

The formation of SC I + III_2, of circa 1400 kDa, in the Δ18-CYB was also clearly seen when the profiles for the $cIII_2$ subunits UQCRC2 and UQCRFS1 were generated (Fig. 3A). As another example on the possibilities of these analyses, we determined that in this case the migration and slicing of lanes A and B were comparable, so we averaged the profiles of both lanes and represented the values of the mean ± SEM in the graphs. This analysis revealed that 'free' $cIII_2$ was also being formed due to the incorporation of the deleted version of MT-CYB. Similar to the Δ4-CYB, the Δ18-CYB cells accumulated significant amounts of the CYC1 and UQCR10 subunits present in stable entities with a range of molecular sizes, although the quantities of these two subunits were much higher in the Δ18-CYB cybrids than in the Δ4-CYB (Figs. 3A and S2A).

Relative abundance quantifications by measuring the AUC of each subunit in the peptide intensity vs. slice number profile graphs, revealed levels of UQCRC1 of around 20% of the control, whereas those of UQCRC2 and UQCRFS1 were approximately 10% (Fig. 3C). In contrast, the amounts of UQCR10 appeared similar to the control (circa 80%), whereas CYC1 levels were ~5-fold higher in the Δ18-CYB mutant (Fig. 3C). Concerning the $cIII_2$ assembly factors, BCS1L was found in the same complex in both cell lines although the amounts were reduced to about half of the control (Fig. 3B and D). MZM1L, the UQCRFS1 chaperone, was equally distributed at low molecular mass and with a similar abundance in the two cell lines (Fig. 3B and D). HIGD1A, although binding to cIV in early stages of assembly, was recently described to have a role in the incorporation of UQCRFS1 into the $cIII_2$ bound to the SC [49]. SILAC-CP of this protein in the Δ18-CYB cybrids compared to the control revealed increased levels, accumulation at low molecular mass positions and impaired binding to cIV (Fig. 3B and D).

The presence of the Δ18-CYB mutation was associated with a dramatic cIV deficiency [26,27], much more profound than that shown by the Δ4-CYB cybrids [21]. This was also reflected in the SILAC-CP analysis (compare Fig. 4A with Fig. S3A). In Δ18-CYB cybrids only peptides corresponding to three cIV subunits, COX4I1 and COX5A (of the 'initial assembly' module) and COX5B, were detected in the mutated

mitochondria and, therefore, found in the common peptide datasets (datasets #2, Fig. 4A). According to this analysis, fully assembled cIV is largely not detected in the Δ18-CYB cybrids. Peptides for three cII subunits (SDHA, B and C) were detected. The amounts of non-fully assembled SDHA were increased in the mutated cells, while the average of SDHB and SDHC showed similar levels of mature cII in the WT and Δ18-CYB cells (Fig. 4B).

In conclusion, SILAC-CP has allowed us to systematically compare two different models of $cIII_2$ deficiency originated from two genetic defects affecting *MT-CYB*. Both models show cI deficiency but a different assembly defect with accumulation of sub-assemblies. The main difference is that there is a residual but still detectable maturation of $cIII_2$ and of cI in the form of SC I + III_2 in the Δ18-CYB, whereas cI assembly is stalled at the pre-cI level in the Δ4-CYB cells, where $cIII_2$ assembly does not occur. Both MT-CYB mutant models accumulate CYC1 and UQCR10 reflecting their stabilization in assembly intermediates formed independently of MT-CYB. Also, SDHA levels are increased and accumulated at lower molecular masses than fully assembled cII in both models. The nature of this phenomenon is still unknown, but it does not result in defective cII activity in neither cell line [21,26]. Remarkably, the cIV deficiency displayed by the Δ18-CYB cells is much more profound than in the Δ4-CYB cybrids. We hypothesised that cIV structural subunits might be trapped within the CYC1 and UQCR10-containing species impairing cIV assembly [21]. Accordingly, the accumulation of CYC1 and UQCR10 is much more exacerbated in the Δ18-CYB in comparison with the Δ4-CYB and this could be the reason why fully assembled cIV levels are so much lower. This possibility needs to be confirmed and will be tested experimentally in the future.

4. Final remarks

CP has provided an important improvement in the study of protein complexes in their native form. However, as it is limited to analysis of a single sample at a time and due to the limitations of mass spectrometry quantitation, changes in protein complex amounts between samples could not be studied. Introduction of SILAC into the CP pipeline has allowed duplexing, reducing the time of sample processing and analysis as well as mitigating technical artefacts created by sequential processing of sample. Furthermore, thanks to the possibility of protein quantification introduced by the SILAC labeling, it has been possible to investigate the relative levels of proteins in the assembled supercomplexes and complexes, as well as their presence and abundance within assembly intermediates in the pathological samples, using their respective isogenic controls as a direct reference.

Data availability

The mass spectrometry data are publicly available in the complexome profiling data resource (CEDAR) [50] website (https://www3.cmbi.umcn.nl/cedar/browse/), with accession numbers CRX19 (for the Δ4-CYB vs. WT data) and CRX26 (data corresponding to the Δ18-CYB cybrids and isogenic WT control).

Declaration of competing interest

The authors declare that they have no known competing financial interests or personal relationships that could have appeared to influence the work reported in this paper.

Acknowledgements

We are very grateful to Prof Valerio Carelli (University of Bologna, Italy) and Dr. Andrea Martinuzzi (IRCCS E.Medea, Padova, Italy) for the Δ18-CYB cell line. We thank Dr. Sara Vidoni (Harvard Medical School, Boston, MA, USA) for her help in setting up the SILAC-CP technique and Drs Shujing Ding and Ian M. Fearnley (Mass Spectrometry Facility, Mitochondrial Biology Unit, Cambridge, UK) for their assistance with mass spectrometry. Funding was provided by MRC core grants MC_UU_00015/4 and MC_UU_00015/5, ERC Advanced Grant FP7-3222424, Association Française contre les Myopathies (AFM) grant 16086, Marie Sklodowska-Curie ITN-REMIX grant (Grant 721757) and by Italian Ministry of Education, University and Research (RFO 2018-2019).

Appendix A. Supplementary data

Supplementary data to this article can be found online at https://doi.org/10.1016/j.bbabio.2021.148395.

References

[1] H. Schagger, K. Pfeiffer, Supercomplexes in the respiratory chains of yeast and mammalian mitochondria, EMBO J. 19 (8) (2000) 1777–1783.
[2] J.A. Letts, L.A. Sazanov, Clarifying the supercomplex: the higher-order organization of the mitochondrial electron transport chain, Nat. Struct. Mol. Biol. 24 (10) (2017) 800–808.
[3] T. Lobo-Jarne, C. Ugalde, Respiratory chain supercomplexes: structures, function and biogenesis, Semin. Cell Dev. Biol. 76 (2018) 179–190.
[4] H. Schagger, Native electrophoresis for isolation of mitochondrial oxidative phosphorylation protein complexes, Methods Enzymol. 260 (1995) 190–202.
[5] P. Klement, L.G. Nijtmans, C. Van den Bogert, J. Houstek, Analysis of oxidative phosphorylation complexes in cultured human fibroblasts and amniocytes by blue-native-electrophoresis using mitoplasts isolated with the help of digitonin, Anal. Biochem. 231 (1) (1995) 218–224.
[6] I. Wittig, H.P. Braun, H. Schagger, Blue native PAGE, Nat. Protoc. 1 (1) (2006) 418–428.
[7] E. Zerbetto, L. Vergani, F. Dabbeni-Sala, Quantification of muscle mitochondrial oxidative phosphorylation enzymes via histochemical staining of blue native polyacrylamide gels, Electrophoresis 18 (11) (1997) 2059–2064.
[8] A. Signes, E. Fernandez-Vizarra, Assembly of mammalian oxidative phosphorylation complexes I-V and supercomplexes, Essays Biochem. 62 (3) (2018) 255–270.
[9] H. Heide, L. Bleier, M. Steger, J. Ackermann, S. Drose, B. Schwamb, M. Zornig, A. S. Reichert, I. Koch, I. Wittig, U. Brandt, Complexome profiling identifies TMEM126B as a component of the mitochondrial complex I assembly complex, Cell Metab. 16 (4) (2012) 538–549.
[10] H.J. Wessels, R.O. Vogel, R.N. Lightowlers, J.N. Spelbrink, R.J. Rodenburg, L. P. van den Heuvel, A.J. van Gool, J. Gloerich, J.A. Smeitink, L.G. Nijtmans, Analysis of 953 human proteins from a mitochondrial HEK293 fraction by complexome profiling, PLoS One 8 (7) (2013), e68340.
[11] H. Giese, J. Meisterknecht, J. Heidler, I. Wittig, Mitochondrial complexome profiling, in: M. Minczuk, J. Rorbach (Eds.), Mitochondrial Gene Expression: Methods and Protocols, Springer US, New York, NY, 2021, pp. 269–285.
[12] C.L. Alston, A.G. Compton, L.E. Formosa, V. Strecker, M. Olahova, T.B. Haack, J. Smet, K. Stouffs, P. Diakumis, E. Ciara, D. Cassiman, N. Romain, J.W. Yarham, L. He, B. De Paepe, A.V. Vanlander, S. Seneca, R.G. Feichtinger, R. Ploski, D. Rokicki, E. Pronicka, R.G. Haller, J.L. Van Hove, M. Bahlo, J.A. Mayr, R. Van Coster, H. Prokisch, I. Wittig, M.T. Ryan, D.R. Thorburn, R.W. Taylor, Biallelic mutations in TMEM126B cause severe complex I deficiency with a variable clinical phenotype, Am J Hum Genet 9 (1) (2016) 217–227.
[13] S. Guerrero-Castillo, F. Baertling, D. Kownatzki, H.J. Wessels, S. Arnold, U. Brandt, L. Nijtmans, The assembly pathway of mitochondrial respiratory chain complex I, Cell Metab. 25 (1) (2017) 128–139.
[14] S. Vidoni, M.E. Harbour, S. Guerrero-Castillo, A. Signes, S. Ding, I.M. Fearnley, R. W. Taylor, V. Tiranti, S. Arnold, E. Fernandez-Vizarra, M. Zeviani, MR-1S interacts with PET100 and PET117 in module-based assembly of human cytochrome c oxidase, Cell Rep. 18 (7) (2017) 1727–1738.
[15] C.L. Alston, J. Heidler, M.G. Dibley, L.S. Kremer, L.S. Taylor, C. Fratter, C. E. French, R.I.C. Glasgow, R.G. Feichtinger, I. Delon, A.T. Pagnamenta, H. Dolling, H. Lemonde, N. Aiton, A. Bjornstad, L. Henneke, J. Gartner, H. Thiele, K. Tauchmannova, G. Quaghebeur, J. Houstek, W. Sperl, F.L. Raymond, H. Prokisch, J.A. Mayr, R. McFarland, J. Poulton, M.T. Ryan, I. Wittig, M. Henneke, R.W. Taylor, Bi-allelic mutations in NDUFA6 establish its role in early-onset isolated mitochondrial complex I deficiency, Am J Hum Genet 103 (4) (2018) 592–601.
[16] J. Van Strien, S. Guerrero-Castillo, I.A. Chatzispyrou, R.H. Houtkooper, U. Brandt, M.A. Huynen, COmplexome Profiling ALignment (COPAL) reveals remodeling of mitochondrial protein complexes in Barth syndrome, Bioinformatics 35 (17) (2019) 3083–3091.
[17] T. Lobo-Jarne, R. Perez-Perez, F. Fontanesi, A. Timon-Gomez, I. Wittig, A. Penas, P. Serrano-Lorenzo, I. Garcia-Consuegra, J. Arenas, M.A. Martin, A. Barrientos, C. Ugalde, Multiple pathways coordinate assembly of human mitochondrial complex IV and stabilization of respiratory supercomplexes, EMBO J. 39 (14) (2020), e103912.
[18] A. Alahmad, A. Nasca, J. Heidler, K. Thompson, M. Olahova, A. Legati, E. Lamantea, J. Meisterknecht, M. Spagnolo, L. He, S. Alameer, F. Hakami, A. Almehdar, A. Ardissone, C.L. Alston, R. McFarland, I. Wittig, D. Ghezzi, R. W. Taylor, Bi-allelic pathogenic variants in NDUFC2 cause early-onset Leigh

syndrome and stalled biogenesis of complex I, EMBO molecular medicine 12 (11) (2020), e12619.
[19] L. Sanchez-Caballero, D.M. Elurbe, F. Baertling, S. Guerrero-Castillo, M. van den Brand, J. van Strien, T.J.P. van Dam, R. Rodenburg, U. Brandt, M.A. Huynen, L.G. J. Nijtmans, TMEM70 functions in the assembly of complexes I and V, Biochim. Biophys. Acta Bioenerg. 2020 (8) (1861) 148202.
[20] C.L. Alston, M.T. Veling, J. Heidler, L.S. Taylor, J.T. Alaimo, A.Y. Sung, L. He, S. Hopton, A. Broomfield, J. Pavaine, J. Diaz, E. Leon, P. Wolf, R. McFarland, H. Prokisch, S.B. Wortmann, P.E. Bonnen, I. Wittig, D.J. Pagliarini, R.W. Taylor, Pathogenic bi-allelic mutations in NDUFAF8 cause Leigh syndrome with an isolated complex I deficiency, Am. J. Hum. Genet. 106 (1) (2020) 92–101.
[21] M. Protasoni, R. Perez-Perez, T. Lobo-Jarne, M.E. Harbour, S. Ding, A. Penas, F. Diaz, C.T. Moraes, I.M. Fearnley, M. Zeviani, C. Ugalde, E. Fernandez-Vizarra, Respiratory supercomplexes act as a platform for complex III-mediated maturation of human mitochondrial complexes I and IV, EMBO J. 39 (3) (2020), e102817.
[22] R. Anand, A.K. Kondadi, J. Meisterknecht, M. Golombek, O. Nortmann, J. Riedel, L. Peifer-Weiß, N. Brocke-Ahmadinejad, D. Schlütermann, B. Stork, T.O. Eichmann, I. Wittig, A.S. Reichert, MIC26 and MIC27 cooperate to regulate cardiolipin levels and the landscape of OXPHOS complexes, Life Sci Alliance 3 (10) (2020).
[23] S.E. Ong, B. Blagoev, I. Kratchmarova, D.B. Kristensen, H. Steen, A. Pandey, M. Mann, Stable isotope labeling by amino acids in cell culture, SILAC, as a simple and accurate approach to expression proteomics, Molecular & cellular proteomics: MCP 1 (5) (2002) 376–386.
[24] S.E. Ong, M. Mann, Stable isotope labeling by amino acids in cell culture for quantitative proteomics, Methods Mol. Biol. 359 (2007) 37–52.
[25] K. Čunátová, D.P. Reguera, M. Vrbacký, E. Fernández-Vizarra, S. Ding, I. M. Fearnley, M. Zeviani, J. Houštěk, T. Mráček, P. Pecina, Loss of COX4I1 Leads to Combined Respiratory Chain Deficiency and Impaired Mitochondrial Protein Synthesis, Cells 10 (2) (2021) 369.
[26] V. Carossa, A. Ghelli, C.V. Tropeano, M.L. Valentino, L. Iommarini, A. Maresca, L. Caporali, C. La Morgia, R. Liguori, P. Barboni, M. Carbonelli, G. Rizzo, C. Tonon, R. Lodi, A. Martinuzzi, V. De Nardo, M. Rugolo, L. Ferretti, F. Gandini, M. Pala, A. Achilli, A. Olivieri, A. Torroni, V. Carelli, A novel in-frame 18-bp microdeletion in MT-CYB causes a multisystem disorder with prominent exercise intolerance, Hum. Mutat. 35 (8) (2014) 954–958.
[27] C.V. Tropeano, S.J. Aleo, C. Zanna, M. Roberti, L. Scandiffio, P. Loguercio Polosa, J. Fiori, E. Porru, A. Roda, V. Carelli, S. Steimle, F. Daldal, M. Rugolo, A. Ghelli, Fine-tuning of the respiratory complexes stability and supercomplexes assembly in cells defective of complex III, Biochim. Biophys. Acta Bioenerg. 2020 (2) (1861) 148133.
[28] C. Lössner, U. Warnken, A. Pscherer, M. Schnölzer, Preventing arginine-to-proline conversion in a cell-line-independent manner during cell cultivation under stable isotope labeling by amino acids in cell culture (SILAC) conditions, Anal. Biochem. 412 (1) (2011) 123–125.
[29] B. Andrews, J. Carroll, S. Ding, I.M. Fearnley, J.E. Walker, Assembly factors for the membrane arm of human complex I, Proc. Natl. Acad. Sci. U. S. A. 110 (47) (2013) 18934–18939.
[30] E. Fernández-Vizarra, G. Ferrín, A. Pérez-Martos, P. Fernández-Silva, M. Zeviani, J. A. Enríquez, Isolation of mitochondria for biogenetical studies: an update, Mitochondrion 10 (3) (2010) 253–262.
[31] H. Schagger, Electrophoretic techniques for isolation and quantification of oxidative phosphorylation complexes from human tissues, Methods Enzymol. 264 (1996) 555–566.
[32] E. Fernandez-Vizarra, M. Zeviani, Blue-native electrophoresis to study the OXPHOS complexes, in: M. Minczuk, J. Rorbach (Eds.), Mitochondrial Gene Expression: Methods and Protocols, Springer US, New York, NY, 2021, pp. 287–311.
[33] R. Perez-Perez, T. Lobo-Jarne, D. Milenkovic, A. Mourier, A. Bratic, A. Garcia-Bartolome, E. Fernandez-Vizarra, S. Cadenas, A. Delmiro, I. Garcia-Consuegra, J. Arenas, M.A. Martin, N.G. Larsson, C. Ugalde, COX7A2L is a mitochondrial complex III binding protein that stabilizes the III2+IV supercomplex without affecting respirasome formation, Cell Rep. 16 (9) (2016) 2387–2398.
[34] E.G. Williams, Y. Wu, P. Jha, S. Dubuis, P. Blattmann, C.A. Argmann, S.M. Houten, T. Amariuta, W. Wolski, N. Zamboni, R. Aebersold, J. Auwerx, Systems proteomics of liver mitochondria function, Science 352(6291) (2016) aad0189.
[35] S. Cogliati, F. Herranz, J. Ruiz-Cabello, J.A. Enríquez, Digitonin concentration is determinant for mitochondrial supercomplexes analysis by BlueNative page, Biochim. Biophys. Acta Bioenerg. 2020 (1) (1862) 148332.
[36] L.G. Nijtmans, N.S. Henderson, I.J. Holt, Blue native electrophoresis to study mitochondrial and other protein complexes, Methods 26 (4) (2002) 327–334.
[37] C. Ramus, A. Hovasse, M. Marcellin, A.M. Hesse, E. Mouton-Barbosa, D. Bouyssie, S. Vaca, C. Carapito, K. Chaoui, C. Bruley, J. Garin, S. Cianferani, M. Ferro, A. Van Dorssaeler, O. Burlet-Schiltz, C. Schaeffer, Y. Coute, A. Gonzalez de Peredo, Benchmarking quantitative label-free LC-MS data processing workflows using a complex spiked proteomic standard dataset, J. Proteome 132 (2016) 51–62.
[38] M.H.D.R. Al Shweiki, S. Mönchgesang, P. Majovsky, D. Thieme, D. Trutschel, W. Hoehenwarter, Assessment of label-free quantification in discovery proteomics and impact of technological factors and natural variability of protein abundance, J. Proteome Res. 16 (4) (2017) 1410–1424.
[39] J.M. Baughman, C.M. Rose, G. Kolumam, J.D. Webster, E.M. Wilkerson, A. E. Merrill, T.W. Rhoads, R. Noubade, P. Katavolos, J. Lesch, D.S. Stapleton, M. E. Rabaglia, K.L. Schueler, R. Asuncion, M. Domeyer, J. Zavala-Solorio, M. Reich, J. DeVoss, M.P. Keller, A.D. Attie, A.S. Hebert, M.S. Westphall, J.J. Coon, D. S. Kirkpatrick, A. Dey, NeuCode proteomics reveals Bap1 regulation of metabolism, Cell Rep. 16 (2) (2016) 583–595.
[40] G.K. Potts, E.A. Voigt, D.J. Bailey, C.M. Rose, M.S. Westphall, A.S. Hebert, J. Yin, J. J. Coon, Neucode labels for multiplexed, absolute protein quantification, Analytical Chemistry 88 (6) (2016) 3295–3303.
[41] L. Zhang, J.E. Elias, Relative protein quantification using tandem mass tag mass spectrometry, Methods Mol. Biol. 1550 (2017) 185–198.
[42] V. Tiranti, P. Corona, M. Greco, J.W. Taanman, F. Carrara, E. Lamantea, L. Nijtmans, G. Uziel, M. Zeviani, A novel frameshift mutation of the mtDNA COIII gene leads to impaired assembly of cytochrome c oxidase in a patient affected by Leigh-like syndrome, Hum. Mol. Genet. 9 (18) (2000) 2733–2742.
[43] I.F. de Coo, W.O. Renier, W. Ruitenbeek, H.J. Ter Laak, M. Bakker, H. Schagger, B. A. Van Oost, H.J. Smeets, A 4-base pair deletion in the mitochondrial cytochrome b gene associated with parkinsonism/MELAS overlap syndrome, Ann.Neurol. 45 (1) (1999) 130–133.
[44] M. Rana, I. de Coo, F. Diaz, H. Smeets, C.T. Moraes, An out-of-frame cytochrome b gene deletion from a patient with parkinsonism is associated with impaired complex III assembly and an increase in free radical production, Ann. Neurol. 48 (5) (2000) 774–781.
[45] L.E. Formosa, M.G. Dibley, D.A. Stroud, M.T. Ryan, Building a complex complex: assembly of mitochondrial respiratory chain complex I, Semin. Cell Dev. Biol. 76 (2018) 154–162.
[46] V. Zara, L. Conte, B.L. Trumpower, Evidence that the assembly of the yeast cytochrome bc1 complex involves the formation of a large core structure in the inner mitochondrial membrane, FEBS J. 276 (7) (2009) 1900–1914.
[47] V. Zara, L. Conte, B.L. Trumpower, Biogenesis of the yeast cytochrome bc1 complex, Biochim.Biophys.Acta 1793 (1) (2009) 89–96.
[48] E. Fernandez-Vizarra, M. Zeviani, Nuclear gene mutations as the cause of mitochondrial complex III deficiency, Front. Genet. 6 (2015) 134.
[49] A. Timon-Gomez, J. Garlich, R.A. Stuart, C. Ugalde, A. Barrientos, Distinct roles of mitochondrial HIGD1A and HIGD2A in respiratory complex and supercomplex biogenesis, Cell Rep. 31 (5) (2020) 107607.
[50] J. van Strien, A. Haupt, U. Schulte, H.P. Braun, A. Cabrera-Orefice, J.S. Choudhary, F. Evers, E. Fernandez-Vizarra, S. Guerrero-Castillo, T.W.A. Kooij, P. Páleníková, M. Pardo, C. Ugalde, I. Wittig, L. Wöhlbrand, U. Brandt, S. Arnold, M.A. Huynen, CEDAR, an online resource for the reporting and exploration of complexome profiling data, bioRxiv (2020) 2020.12.11.421172.